Journal of Inorganic Biochemistry 198 (2019) 110751

Contents lists available at ScienceDirect

Journal of Inorganic Biochemistry

journal homepage: www.elsevier.com/locate/jinorgbio

Ru(II) complexes containing uracil nucleobase analogs with cytotoxicity against tumor cells

Rodrigo S. Correa[a,*], Larissa M. Bomfim[b], Katia M. Oliveira[a], Diogo R.M. Moreira[b], Milena B.P. Soares[b], Javier Ellena[c], Daniel P. Bezerra[b], Alzir A. Batista[d,e,**]

[a] Departamento de Química, ICEB, Universidade Federal de Ouro Preto, CEP 35400-000 Ouro Preto, MG, Brazil
[b] Instituto Gonçalo Moniz, Fundação Oswaldo Cruz (IGM-Fiocruz/BA), CEP 40296-710 Salvador, Bahia, Brazil
[c] Instituto de Física de São Carlos, Universidade de São Paulo, Caixa Postal 369, CEP 13560-970 São Carlos, SP, Brazil
[d] Departamento de Química, Universidade Federal de São Carlos - UFSCar, Rodovia Washington Luiz, KM 235 CP 676, CEP 13561-901 São Carlos, SP, Brazil
[e] Instituto de Química, Universidade Federal de Goiás - UFG, CEP 74690-900 Goiânia, GO, Brazil

ARTICLE INFO

Keywords:
Ruthenium(II) complexes
Thiouracil ligands
DNA
BSA
Antitumor

ABSTRACT

We report on chemistry and cytotoxic studies of four new ruthenium (II) complexes containing uracil derivatives. All compounds are neutral, presenting the formula $[Ru(PPh_3)_2(2TU)_2]$ (**1**), $[Ru(PPh_3)_2(6m2TU)_2]$ (**2**), [Ru(dppb)$(2TU)_2$] (**3**) and [Ru(dppb)$(6m2TU)_2$] (**4**), where PPh_3 = triphenylphosphine; dppb = 1,4-*bis*(diphenylphosphino)butane, 2TU = 2-thiouracil and 6m2TU = 6-methyl-2-thiouracil. They were characterized using NMR, UV–vis and IR spectroscopies, microanalytical analysis and mass spectrometry. Furthermore, the crystal structures of **1–4** were determined by single-crystal X-ray diffraction. The coordination of 2-thiouracil derivatives with ruthenium increases regions able to carry out hydrogen bonds with the biological targets, such as DNA. We evaluated the interaction of the complexes with DNA by UV/Vis spectrophotometric titration, and as a result, the values of DNA-binding constants are in the range of $0.8–1.8 \times 10^4\ M^{-1}$. Moreover, the interaction of the complexes with BSA was investigated. *In vitro*, activities against B16-F10 (mouse melanoma), HepG2 (human hepatocellular carcinoma), HL-60 (human promyelocytic leukemia) and K562 (human chronic myelocytic leukemia) and non-tumor cells: PBMC (human peripheral blood mononuclear cells activated with concanavalin A – human lymphoblast) were carried out. Cytotoxicity assays revealed that complexes (**2**) and (**4**) present biological activity against tumor cells comparable with oxaliplatin, the reference platinum drug, revealing that they are promising molecules for developing new antitumor compounds.

1. Introduction

Over the last decade, considerable interest has been expressed in metallodrugs based on ruthenium(II) given that a number of compounds present promising pharmacological properties, including anticancer [1], antibacterial [2] and antiparasitic [3] ones. A key strategy used by many research groups has been to select a suitable target for specific diseases. For instance, concerning cancer, either DNA or protein (*i.e.* topoisomerases, kinases) can be chosen to understand the mechanism of action [4–6], aiming to design selective molecules that bind tightly to the biological target. Ruthenium compounds are known as promising anticancer agents, which are well-exemplified by KP1339, RAPTA and staurosporine-like compounds [4–6]. Recent studies have shown that bioligand-coordinated Ru(II) complexes potentially inhibit cancer [7–12], bacteria [13–17] and parasite [18,19] proliferation. As part of this ongoing long-term study to improve the pharmacological potential of mononuclear and octahedral Ru(II)-complexes, we are interested in the application of nucleobase analogs as potential ligands for ruthenium coordination. Six-coordinate metal complexes present additional geometric possibilities compared with four-coordinate carbon. This makes this class of compound an attractive approach for developing new active species [20]. Moreover, bioligands such as nucleobase analogs, for instance as 2-thiouracil (2TU) and 6-methyl-2-thiouracil (6m2TU), have a great potential for designing anticancer Ru(II)-complexes because they play a role in recognizing nuclear DNA, especially for non-canonical DNA sequences in aberrant and mutated cells, best

* Corresponding author.
** Correspondence to: A.A. Batista, Departamento de Química, Universidade Federal de São Carlos - UFSCar, Rodovia Washington Luiz, KM 235 CP 676, CEP 13561-901 São Carlos, SP, Brazil.
E-mail addresses: rodrigocorrea@ufop.edu.br (R.S. Correa), daab@ufscar.br (A.A. Batista).

https://doi.org/10.1016/j.jinorgbio.2019.110751
Received 26 February 2019; Received in revised form 22 May 2019; Accepted 5 June 2019
Available online 09 June 2019
0162-0134/

observed in cancer cells [21]. However, Ru(II)-complexes with only nucleobase ligands may present poor lipophilicity, limiting their cell permeation. To overcome this, inserting highly inert and lipophilic phosphine co-ligands is a powerful strategy in providing cell-permeable Ru(II)-complexes [22,23]. To date, most studies of anticancer metal-complexes have been conducted for *N,O*-coordinated nucleobase ligands and mimetics [24], while much less studies have been devoted to underlying the *N,S*-coordinated sites [12,25].

Moreover, the metal interaction with the nucleobase has kindled great interest in biochemistry despite the biological importance of nucleobases. From the structural point of view, this molecular system has become interesting because of the many coordination modes and the ability to form strong hydrogen bonds, allowing the base pairing. In particular, nucleobases are molecules with many possibilities of binding, including nitrogen and oxygen atoms of pyrimidine and purine moiety, which allow different reactivity, depending essentially on the metal ion with a "*hard*" or "*soft*" acidic character [26]. In DNA, "*hard*" metal ions interact preferentially with the phosphate group, influencing the stabilization of the double helix. On the other hand, "*soft*" metal ions may interact with the nitrogen of purine or pyrimidine moiety, and consequently, destabilize the DNA structure and base pairing. Thus, the use of thiouracil ligands due to the "*soft*" base characteristic of sulfur may be an alternative to form stable complexes with "*soft*" or 'borderline" acid metals such as Ru(II) [26].

Therefore, as part of our ongoing efforts to improve the biological activity of Ru(II)-based complexes, herein we used uracil nucleobase analogs as ligands. Nucleobase analogs, such as 2-thiouracil (2TU) and 6-methyl-2-thiouracil (6m2TU), have a great potential for designing anticancer Ru(II)-complexes because these ligands can play a role in recognizing nuclear DNA, especially for non-canonical DNA sequences in aberrant and mutated cells, best observed in cancer cells. In order to investigate the reactivity of Ru(II) ions towards the nucleobase, we used uracil derivatives as ligands that may behave differently, depending on the nature of the metal ion. Scheme 1 (top) shows the chemical structure of uracil, as well as atom labeling, highlighting two ligands studied here: 2-thiouracil (2TU) and 6-methyl-2-thiouracil (6m2TU). Several metal complexes present monodentate coordination mode with 2-thiouracil derivatives, occurring through the N1 atom (*e.g.* Cu(I) complex) [27], N3 atom (*e.g.* Pd(II), Hg(II) complexes) [28,29] S atom (*e.g.* Ru(II), Cu(I), Au(I) complexes) [30–32] or O atom (*e.g.* Co(II), Ni(II), Mn(II) Zn(II) complexes) [33–35].

At the bottom of Scheme 1, the coordination modes of these ligands as bidentate are highlighted. There are at least four possibilities of coordination as bidentate (a-d) for both 2TU and 6m2TU ligands. Some of these coordination modes were studied by Lusty and collaborators [36], in which they discussed the coordination represented in (a) and (b) upon the presence of platinum and rhodium centers, respectively, which are in fact the two most classical coordination modes for this class of ligands. Complexes with Pd(II) and Zn(II) also exhibit the coordination mode (a) [28,37], while the coordination mode (b) occurs for Co(II) complexes [38]. To date, possibility (c) was not observed for thiouracil derivatives, occurring in an osmium/uracil complex [39]. The coordination mode viewed in (d) is observed for Ru(II) complex with 2,2′-bipyridine (bipy) [40] and tin(IV) complexes [41]. Focusing on Ru(II) complexes with 2-thiouracil derivatives, only the coordination modes (d) in the $[\{(bipy)_2Ru\}_2(\mu\text{-}6m2TU)]ClO_4$ with 6m2TU as a versatile ambidentate ligand, and monodentated directly linked through the sulfur atom in the $[Ru(\eta^6\text{-}p\text{-}cymene)(2TU)Cl_2]$ were reported, depending on the starting complexes used for synthesis. To the best of our knowledge, the structural and biological studies were not explored for ruthenium(II)/phosphinic-based complexes containing 2-thiouracil derivatives.

Therefore, this paper presents the synthesis and characterization of four new complexes containing 2-thiouracil derivative as ligands that were obtained from the $[RuCl_2(PPh_3)_3]$ and $[RuCl_2(PPh_3)(dppb)]$ complexes, as starting material, where PPh_3 = triphenylphosphine; dppb = 1,4′-*bis*(diphenylphosphino)butane. The complexes were fully characterized by physical and chemical techniques, especially by X-ray crystallography. Moreover, the DNA-binding studies by UV/Vis spectrophotometric titration, interaction with BSA by fluorescence technique and the *in vitro* study of cytotoxicity against B16-F10 (mouse melanoma), HepG2 (human hepatocellular carcinoma), HL-60 (human promyelocytic leukemia), K562 (human chronic myelocytic leukemia) and non-tumor cell PBMC (human peripheral blood mononuclear cells activated with concanavalin A – human lymphoblast) were evaluated.

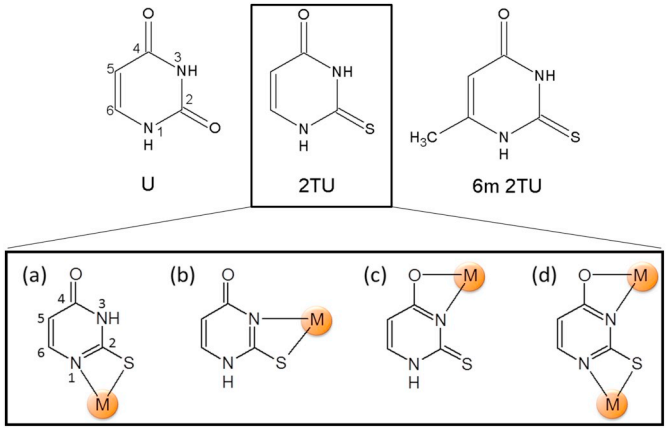

Scheme 1. (Top) Structure of uracil (U) and the two ligands: 2-thiouracil (2TU) and 6-methyl-2-thiouracil (6m2TU), as well as numbered atoms. (Bottom) Representation of coordination binding sites for 2TU ligand. The same trend can also be expected for uracil and 6m2TU ligands.

2. Materials and methods

2.1. Materials and physical measurements

The chemicals used were of reagent grade or comparable purity. $RuCl_3.3H_2O$, PPh_3 (triphenylphosphine), dppb (1,4′-*bis*(diphenylphosphino)butane), bipy (2,2′-bipyridine), 2TU (2-thiouracil) and 6m2TU (6-methyl-2-thiouracil) were purchased from Sigma-Aldrich (St. Louis, MO, USA) and used as supplied. Elemental analyses were carried out on an EA 1108 FISONS Instrument CHNS microanalyzer. Conductivity values were obtained at room temperature using 10^{-3} M solutions of the complexes in DMSO (dimethylsulfoxide) by using a MeterLab CDM2300 instrument. The IR spectra were recorded on a FT-IR Bomem-Michelson 102 spectrometer in the 4000–200 cm^{-1} region, using CsI pellets (Fig. S1). The UV–Vis spectra of the complexes were recorded in CH_2Cl_2 (dichloromethane) on a Hewlett Packard diode array–8452A. Cyclic voltammetry (CV) experiments were performed in an electrochemical analyzer BAS, model 100B and carried out at room temperature. The typical conditions were: CH_2Cl_2 containing 0.10 mol L^{-1} Bu_4NClO_4 (TBAP) as the supporting electrolyte, using a one-compartment cell, where both working and auxiliary electrodes are stationary Pt foils, and the reference electrode was Ag/AgCl, 0.10 M TBAP in CH_2Cl_2. Under these conditions, the ferrocene (Fc) is oxidized at 0.43 V (Fc^+/Fc). High resolution mass spectra of complexes **1–4** were obtained by direct infusion in a MicroTof-Q II Bruker Daltonics Mass Spectrometer (Le) in the positive ion mode, using methanol/acetonitrile mixture (LC/MS grade from Honeywell/B&*J* Brand). All complexes were studied using the NMR technique. The ^1H, $^{31}P\{^1H\}$ and ^{13}C NMR spectra were recorded on a Bruker DRX 400 MHz using TMS (Tetramethylsilane) as a reference and solvent DMSO-d_6 for the complexes. The ^{31}P chemical shifts are reported in relation to H_3PO_4, 85%. The spectra are shown in the Supplementary information (Figs. S1-S25).

2.2. Synthesis of the complexes

$[Ru(PPh_3)_2(2TU)_2]$ (**1**) and $[Ru(PPh_3)_2(6m2TU)_2]$ (**2**). In a Schlenk flask, 0.25 mmol of 2TU or 6m2TU ligands were dissolved in ethanol (50 mL) solution containing 20 μL of triethylamine (Et_3N). Afterwards, 100 mg (0.12 mmol) of the $[RuCl_2(PPh_3)_3]$, obtained according to the literature [42], solubilized in 50 mL of dichloromethane, was added to the reaction flask. The mixture was kept under stirring and reflux for 12 h. Then, the volume of the solution was reduced to *ca.* 4 mL and yellow solids were formed. The solid was collected by filtration, washed with ethanol, diethyl ether and dried under vacuum to yield 76 mg (83%) of complex (**1**) and 70 mg (74%) of complex (**2**).

$[Ru(dppb)(2TU)_2]$ (**3**) and $[Ru(dppb)(6m2TU)_2]$ (**4**). In a Schlenk flask, 0.35 mmol of the ligands 2TU or 6m2TU were dissolved in a methanol (50 mL) solution containing 20 μL of triethylamine (Et_3N). Afterwards, 50 mL of dichloromethane solution containing 100 mg (0.12 mmol) of the $[RuCl_2(PPh_3)(dppb)]$ precursor was added to the reaction media. The mixture was maintained under stirring and reflux for 12 h. Then, the volume of the solution was reduced to c.a 4 mL and yellow solids were formed. The solid was collected by filtration, washed with methanol, diethyl ether and dried under vacuum to yield 75 mg (82%) of complex (**3**) and 69 mg (73%) of complex (**4**).

*Complex (**1**)*. Anal. Calc. for $[RuC_{44}H_{36}N_4O_2P_2S_2]$: exp. (calc) 59.90 (59.92); H, 4.21 (4.34); N, 6.28 (6.36); S, 7.55 (7.27) %. Molar conductance ($\Omega^{-1}cm^2mol^{-1}$, DMSO) 6.9. IR (cm^{-1}): 3200, 3053, 2955, 2924, 1688, 1637, 1570, 1481, 1458, 1433, 1311, 1273, 1186, 1159, 1088, 1020, 1001, 814, 744, 717, 696, 619, 538, 507, 460, 420, 311, ^{31}P NMR (162 MHz, DMSO-d_6, 298 K) δ(ppm): 52.8 (s); ^1H NMR (400 MHz, DMSO-d_6, 298 K) δ(ppm): 12.3 (2H, N—H), 7.3–7.0 (30H aromatic hydrogen atoms of PPh_3); 6.9 (2H, C_6—H of 2TU); 5.4 (2H, C_5—H of 2TU). $^{13}C\{^1H\}$ NMR (125.74 MHz, DMSO-d_6, 298 K) δ(ppm): 179.0 (C=S); 160.8 (C=O); 148.3 (C6 of 2TU), 108.3 (C5 of 2TU); 135–127 (36C of PPh_3). UV–Vis (DMSO, 2.5×10^{-5} M): λ/nm (ε/$mol^{-1}Lcm^{-1}$) 298 (14300), 342 (8570).

*Complex (**2**)*. Anal. Calc. for $RuC_{46}H_{40}N_4O_2P_2S_2.2H_2O$: exp. (calc) C 58.75 (58.53), H 4.60 (4.70), N 5.65 (5.93), S 6.79(6.79) %. Molar conductance ($\Omega^{-1}cm^2mol^{-1}$, DMSO) 5.55. IR (cm^{-1}) 3175, 3059, 2972, 2835, 2681, 1659, 1640, 1585, 1574, 1500, 1481, 1443, 1431, 1394, 1364, 1313, 1209, 1240, 1120, 1140, 1161, 1092, 1030, 993, 966, 817, 748, 698, 680, 598, 542, 522, 460, 420, 322. $^{31}P\{^1H\}$ NMR (162 MHz, DMSO-d_6, 298 K): δ(ppm) 50.6 (s); ^1H NMR (400 MHz, DMSO-d_6, 298 K) δ(ppm): 11.9 (2H, N—H), 7.3–7.0 (30H aromatic hydrogen atoms of PPh_3); 5.2 (2H, C_5—H of 6m2TU); 1.9 (6H, CH_3 of 6m2TU). $^{13}C\{^1H\}$ NMR (125.74 MHz, DMSO-d_6, 298 K) δ(ppm): 179.2 (C=S); 163.7 (C=O); 160.2 (C6 of 2TU), 106.8 (C5 of 2TU); 136–127 (36C of PPh_3). UV–Vis (DMSO, 2.2×10^{-5} M): λ/nm (ε/$mol^{-1}Lcm^{-1}$) 298 (12000), 350 (96000).

*Complex (**3**)*. Anal. Calc. for $[RuC_{36}H_{34}N_4S_2P_2]$: exp. (calc) 55.08 (55.16); H, 4.70 (4.63); N, 7.28 (7.15); S, 8.07 (8.18) %. Molar conductance ($\Omega^{-1}cm^2mol^{-1}$, DMSO) 5.1. IR (cm^{-1}): 3196, 3053, 2924, 3074, 2866, 1674, 1657, 1639, 1568, 1495, 1454, 1433, 1311, 1275, 1159, 1144, 1094, 1018, 999, 970, 899, 815, 741, 717, 698, 650, 580, 515, 461, 424, 357. $^{31}P\{^1H\}$ NMR (162 MHz, DMSO-d_6, 298 K): δ(ppm) 51.4 (s); ^1H NMR (400 MHz, DMSO-d_6, 298 K) δ(ppm): 12.1 (2H, N—H), 7.5–7.0 (20H aromatic hydrogen atoms of dppb); 6.9 (2H, C_6—H of 2TU); 5.4 (2H, C_5—H of 2TU); 2.8–1.5 (8H, CH_2 of dppb). $^{13}C\{^1H\}$ NMR (125.74 MHz, DMSO-d_6, 298 K) δ(ppm): 179.2 (C=S); 160.8 (C=O); 149.0 (C6 of 2TU), 107.8 (C5 of 2TU); 138–127 (24C of dppb); 30–23 (4C of dppb). UV–Vis ($DMSO_2$, 6×10^{-5} M): λ/nm (ε/$mol^{-1}Lcm^{-1}$) 298 (9980), 338 (7300).

*Complex (**4**)*. Anal. Calc. for $[RuC_{38}H_{38}N_4O_2P_2S_2]$: exp. (calc) 56.60 (56.21); H, 4.70 (4.91); N, 6.76 (6.90); S, 7.58 (7.90) %. Molar conductance ($\Omega^{-1}cm^2mol^{-1}$, DMSO) 6.2. IR (cm^{-1}): 3175, 3053, 2922, 3074, 2853, 1645, 1587, 1574, 1495, 1483, 1448, 1433, 1396, 1361, 1228, 1207, 1190, 1094, 1041, 995, 960, 889, 820, 748, 741, 698, 660, 619, 594, 570, 517, 511, 463, 422, 322. $^{31}P\{^1H\}$ NMR (162 MHz, DMSO-d_6, 298 K): δ(ppm) 49.5 (s); ^1H NMR (400 MHz, DMSO-d_6, 298 K) δ(ppm): 11.7 (2H, N—H), 7.5–7.0 (20H aromatic hydrogen atoms of dppb); 5.2 (2H, C_5—H of 6m2TU); 3.0–1.6 (8H, CH_2 of dppb). $^{13}C\{^1H\}$ NMR (125.74 MHz, DMSO-d_6, 298 K) δ(ppm): 178.3 (C=S); 163.7 (C=O); 153.0 (C6 of 2TU), 106.0 (C5 of 2TU); 140–127 (24C of dppb); 30–18 (4C of dppb). UV–Vis (DMSO, 4×10^{-5} M): λ/nm (ε/$mol^{-1}Lcm^{-1}$) 298 (10100), 350 (8040).

2.3. X-ray structure determination

Single crystals of complexes **1–4** were grown from diethyl ether diffusion into a methanol/dichloromethane solution of complex at room temperature (293 K). X-ray diffraction experiments were carried out at room temperature using a suitable crystal mounted on glass fiber, and positioned on the goniometer head. Intensity data were measured on an Enraf–Nonius Kappa-CCD diffractometer with graphite monochromated MoKα radiation (λ = 0.71073 Å). The structures were solved by the Direct method using SHELXS-97 and refined using the software SHELXL-97 [43]. In all complex structures, the Gaussian method was used for the absorption corrections [44]. Non-hydrogen atoms of the complexes were unambiguously located, and a full-matrix, least-square refinement of these atoms with anisotropic thermal parameters was carried out. In all ligands of complexes **1–4**, the aromatic C—H hydrogen atoms were positioned stereochemically and were refined with fixed individual displacement parameters [$U_{iso}(H) = 1.2\ U_{eq}(Csp^2)$] using a riding model with aromatic rings. Moreover, C—H bond lengths were fixed of 0.93 Å. Methylene groups of the dppb ligand were also set as isotropic with a thermal parameter 20% greater than the equivalent isotropic displacement parameter of the atom to which each one was bonded and C—H bond lengths were fixed of 0.97 Å.

Tables were generated by WinGX [45] and the structure representations by MERCURY [46]. The CrystalExplorer program [47] was used to generate the Hirshfeld surfaces and the fingerprint plot of 1–4 (Fig. S26). The Hirshfeld surfaces define the intermolecular environment of molecules within the crystal of each complex, allowing us to explore its intermolecular contacts in a crystalline structure. The fingerprint plot or 2D-fingerprint graphics was constructed by the *de versus di* plot (*de* = external distance is defined as the distance between the calculated Hirshfeld surface and the nearest atom of an adjacent molecule; *di* = internal distance is the distance between the nearest nucleus internal and the calculated Hirshfeld surface). Relationships between crystal packing pattern and molecular geometry are understood by analyzing parameters present in the Hirshfeld fingerprint plots. The 2D-fingerprint also provides the percentage of each intermolecular contact occurring in the complex structure.

2.4. CT-DNA binding experiments

2.4.1. Spectroscopic titrations

Calf thymus DNA solution (CT-DNA, purchased from Sigma-Aldrich) was prepared in a Tris-HCl buffer (5 mM Tris-HCl, pH 7.2). A solution of CT-DNA in the buffer gave a ratio of UV absorbance at 260 and 280 nm of about 1.8:1, indicating that the solution is protein-free. The concentration of CT-DNA was measured from its absorption intensity at 260 nm using the molar absorption coefficient value of 6600 $M^{-1}\,cm^{-1}$. The solution of ruthenium complexes used in the experiments was prepared in a Tris-HCl buffer containing 5% DMSO. For the titration experiment, different concentrations of the CT-DNA were used while the ruthenium complex was 25 μM. A sample correction was made for DNA absorbance and the spectra were recorded after solution equilibration for 2 min. The intrinsic equilibrium binding constant (K_b) of the complexes to CT-DNA was obtained using the expression proposed by Wolfe et al. [48]. Changes in the absorption intensity increasing concentration of CT-DNA was monitored and analyzed by regression analysis.

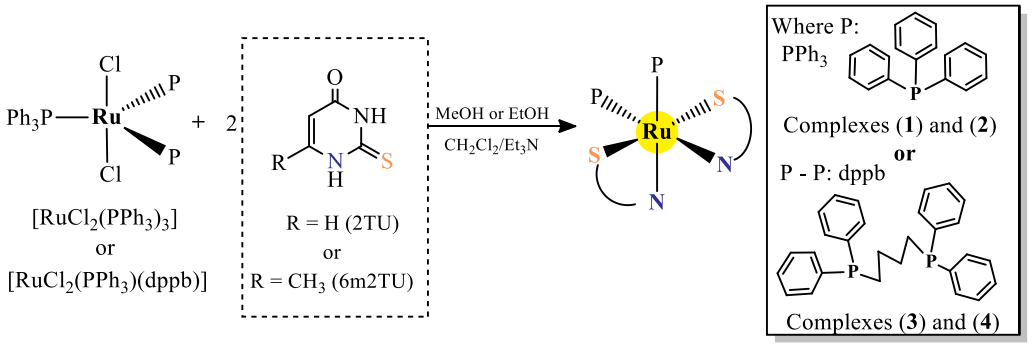

Scheme 2. Synthetic route used to obtain the ruthenium complexes (**1–4**).

Table 1
$^{31}P\{^{1}H\}$ NMR and cyclic voltammetry data for complexes **1–4.**

Complexes	$^{31}P\{^{1}H\}$, δ (ppm)	Epa[a] (mV)	E½ (mV)	|Ipa/Ipc|
(**1**)	52.8	922	839	0.96
(**2**)	50.6	880	727	1.00
(**3**)	51.4	765	697	0.97
(**4**)	49.5	775	682	0.99

[a] Electrolyte: TBAP 0.1 mol L^{-1}, Solvent: CH_2Cl_2 and Reference: Ag/AgCl.

2.5. Bovine serum albumin binding experiment

The protein binding experiment was carried out using the bovine serum albumin (BSA, 2.5 μM) in a Tris-HCl buffer by fluorescence quenching of tryptophan residues. Complexes (**1–4**) were used as quenchers with increasing concentration. The fluorescence spectra were performed by excitation at 280 nm and emission at 340 nm on a SpectraMax M3 at 298 and 310 K, using an opaque 96-well plate.

2.6. Cells

The tumor cell lines B16-F10 (mouse melanoma), HepG2 (human hepatocellular carcinoma), K562 (human chronic myelocytic leukemia) and HL-60 (human promyelocytic leukemia) were obtained from the American Type Culture Collection (ATCC, Manassas, VA, USA), and were cultured as recommended by ATCC. All cell lines were tested for mycoplasma using the Lookout® Mycoplasma qPCR detection kit (Sigma-Aldrich) to validate the use of cells free from contamination. Peripheral blood mononuclear cells (PBMCs) were isolated *via* a standard protocol using a Ficoll density gradient in GE Ficoll-Paque Plus from heparinized blood collected from 20- to 35-year-old, non-smoker healthy donors with informed consent. The PBMCs were cultured in the RPMI 1640 medium supplemented with 20% fetal bovine serum, 2 mM glutamine, and 50 μg/mL gentamycin at 37 °C with 5% CO_2. ConA (10 μg/mL) was added at the beginning of the culture, and the cells were treated with the test drugs after 24 h. The Research Ethics Committee of the Oswaldo Cruz Foundation (Salvador, Bahia, Brazil) approved the experimental protocol (number 031019/2013).

Table 2
Crystal data and structure refinement parameters obtained for **1–4**.

Complex	**1**	**2**	**3**	**4**
Empirical formula	$[RuC_{44}H_{36}N_4O_2P_2S_2]$	$[RuC_{46}H_{40}N_4O_2P_2S_2]$ $2CH_3OH$	$[RuC_{36}H_{34}N_4O_2P_2S_2]$ CH_2Cl_2	$[RuC_{38}H_{38}N_4O_2P_2S_2]$
Formula weight	879.90	972.03	885.26	809.85
Crystal system	Orthorhombic	Monoclinic	Monoclinic	Monoclinic
Space group	$P2_1cn$	$P2_1$	C2/c	C2/c
Unit cell dimensions (Å, °)	a = 17.529(6)	a = 10.0940(4)	a = 20.9432(12)	a = 33.6253(12)
	b = 13.314(4)	b = 15.4510(12)	b = 32.860(4)	b = 11.2764(4)
	c = 18.311	c = 14.8220(7)	c = 14.2589(8)	c = 20.2448(6)
		β = 97.157(3)	β = 122.894(2)	β = 104.116(2)
Volume ($Å^3$)	4273.4 (4)	2293.7(2)	8239.7(13)	7444.1(4)
Z	4	2	8	8
Density calculated (Mg/m^3)	1.368	1.407	1.427	1.445
μ (mm^{-1})	0.580	0.551	0.727	1.445
F(000)	1800	1004	3620	3328
Crystal size (mm^3)	0.07 × 0.19 × 0.40	0.03 × 0.15 × 0.19	0.08 × 0.14 × 0.18	0.10 × 0.13 × 0.21
θ range (°)	3.26 to 25.76°	2.91 to 26.36°	3.15 to 26.39	2.93 to 26.73
Index ranges	0 ≤ h ≤ 21.	−12 ≤ h ≤ 12.	−0 ≤ h ≤ 26.	−42 ≤ h ≤ 42.
	0 ≤ k ≤ 15.	−19 ≤ k ≤ 19.	−0 ≤ k ≤ 19.	−14 ≤ k ≤ 14.
	−22 ≤ l ≤ 22	−18 ≤ l ≤ 18	−17 ≤ l ≤ 14	−25 ≤ l ≤ 25
Reflections collected	7636	16,151	8426	26,509
Independent reflections	4037 [R(int) = 0.0254]	8937 [R(int) = 0.0383]	8426 [R(int) = 0.0498]	7847[R(int) = 0.0319]
Completeness to θ (%)	95.5	99.4%	99.4	99.2
Data / restraints / parameters	4037 / 1 / 496	8937 / 1 / 549	8426 / 0 / 451	7847 / 0 / 444
Goodness-of-fit on F^2	1.062	1.067	1.050	1.061
Final R indices [I > 2sigma(I)]	R_1 = 0.0360.	R_1 = 0.0484.	R_1 = 0.0567, wR_2 = 0.1508	R_1 = 0.0369.
	wR_2 = 0.0920	wR_2 = 0.1049		wR_2 = 0.0928
R indices (all data)	R_1 = 0.0392.	R_1 = 0.0618.	R_1 = 0.0854, wR_2 = 0.1655	R_1 = 0.0486.
	wR_2 = 0.0946	wR_2 = 0.1107		wR_2 = 0.0974
Flack parameter	0.07(3)	0.00(2)	–	–
$\Delta\rho_{max.}$ e $\Delta\rho_{min.}$ (e. $Å^{-3}$)	0.467 and − 0.505	0.650 and − 0.979	0.860 and − 0.742	0.399 and − 0.733

Table 3
Representation of the main bond lengths for complexes **1–4** and the free thiouracil derivatives [55].

Bond	(1)	(2)	(3)	(4)	2TU	6m2TU
Ru1-N1	2.147(4)	2.212(4)	2.164(5)	2.2075(19)	–	–
Ru1-N1′	2.172(4)	2.191(4)	2.162(4)	2.205(2)	–	–
Ru1-P1	2.3476(13)	2.3148(13)	2.2808(15)	2.2754(7)	–	–
Ru1-P2	2.3139(14)	2.3120(13)	2.2725(15)	2.205(2)	–	–
Ru1-S2	2.4539(11)	2.4195(13)	2.4235(15)	2.4250(6)	–	–
Ru1-S2′	2.4381(12)	2.4272(13)	2.4502(15)	2.4284(6)	–	–
S2-C2	1.719(5)	1.701(5)	1.709(6)	1.706(3)	1.684	1.675
N1-C2	1.353(6)	1.335(6)	1.334(7)	1.328(3)	1.352	1.357
N1-C6	1.346(7)	1.372(6)	1.348(8)	1.365(3)	1.371	1.378
N3-C2	1.355(5)	1.371(6)	1.352(7)	1.352(3)	1.356	1.359
N3-C4	1.404(7)	1.378(6)	1.400(8)	1.383(3)	1.395	1.389
O4-C4	1.243(6)	1.259(6)	1.236(7)	1.240(3)	1.232	1.233
C4-C5	1.425(8)	1.406(8)	1.419(10)	1.412(4)	1.444	1.438
C5-C6	1.381(8)	1.373(8)	1.355(9)	1.361(4)	1.352	1.363

2.7. In vitro cytotoxic activity assay

Cell growth was quantified using the alamar blue assay as previously described [49]. Cells were seeded into 96-well plates for all experiments (0.7×10^5 cells/mL for adherent cells or 0.3×10^6 cells/mL for cells suspended in 100 µL of medium). After 24 h, the compounds (0.19–25.0 µg/mL), dissolved in dimethyl sulfoxide (DMSO, Sigma Chemical Co.), were added to each well and incubated for 72 h. As positive controls, oxaliplatin (Sigma-Aldrich) and doxorubicin (doxorubicin hydrochloride, Laboratory IMA S.A.I·C) were used. The negative controls received the vehicle used for diluting the tested compounds (0.5% DMSO). Four (for cell lines) or 24 (for PBMCs) h before the end of incubation, 20 µL of a stock solution (0.312 mg/mL) of alamar blue (resazurin, Sigma–Aldrich Co) was added to each well. Absorbance was measured using a SpectraMax 190 multiplate reader at 570 nm and 600 nm.

2.8. Internucleosomal DNA fragmentation and cell cycle distribution

Cells were harvested in a permeabilization solution (0.1% triton X-100, 2 µg/mL propidium iodide, 0.1% sodium citrate and 100 µg/mL RNAse, all from Sigma-Aldrich Co.) and incubated in the dark for 15 min at room temperature. Cell fluorescence was measured by flow cytometry. At least 10^4 events were recorded per sample using a BD LSRFortessa cytometer, as well as BD FACSDiva Software (BD Biosciences, San Jose, CA, USA) and Flowjo Software 10 (Flowjo LCC, Ashland, OR, USA). The cellular debris was omitted from the analysis.

2.9. Statistical analysis

Data are presented as half-maximal inhibitory concentration (IC_{50}) values and their 95% confidence intervals were obtained *via* nonlinear regression from three independent experiments performed in duplicate. The statistical analysis was carried out using the GRAPHPAD software (Intuitive Software for Science).

3. Results and discussion

The chemical reactivity of the 2-thiouracil derivatives in the presence of the precursors $[RuCl_2(PPh_3)_3]$ and $[RuCl_2(PPh_3)(dppb)]$ was investigated. As a result, the neutral complexes $[Ru(PPh_3)_2(2TU)_2]$ (**1**), $[Ru(PPh_3)_2(6m2TU)_2]$ (**2**), $[Ru(dppb)(2TU)_2]$ (**3**) and $[Ru(dppb)(6m2TU)_2]$ (**4**), containing the monoanionic 2-thiouracil derivatives as chelated ligand were isolated at mild conditions, as summarized in the procedure illustrated in Scheme 2.

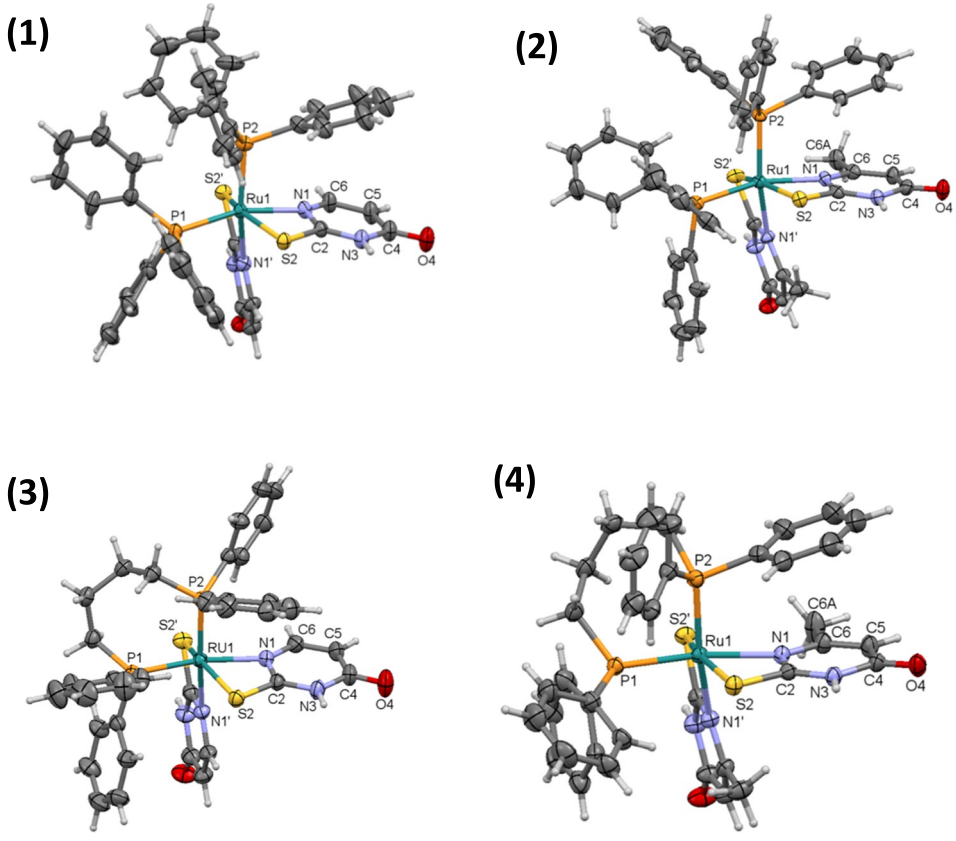

Fig. 1. Crystal structures of complexes **1–4**, presenting the main atoms labeled and thermal ellipsoids drawn at the 30% probability level.

Table 4
Distance (Å) and angle (°) for H-bonds of **1–4.**

Complex	*D*–H···A	*D*–H	H···A	*D*···A	*D*–H···A
1	N3–H3···O4′	0.86	1.95	2.806(6)	175
	N3′–H3′···O4	0.86	1.95	2.747(5)	154
2	N3–H3···O4′	0.86	1.95	2.809(6)	176
	N3′–H3′···O1s	0.86	1.97	2.818(8)	171
	O1s–H1w···O2s	0.82	1.95	2.762(11)	173
	O2s–H2w···O4	0.82	1.88	2.698(9)	173
3	N3–H3···O4	0.86	1.94	2.769(9)	160
	N3′–H3′···O4′	0.86	1.92	2.773(8)	174
4	N3–H3···O4	0.86	1.87	2.725(3)	173
	N3′–H3′···O4′	0.86	1.93	2.743(8)	156

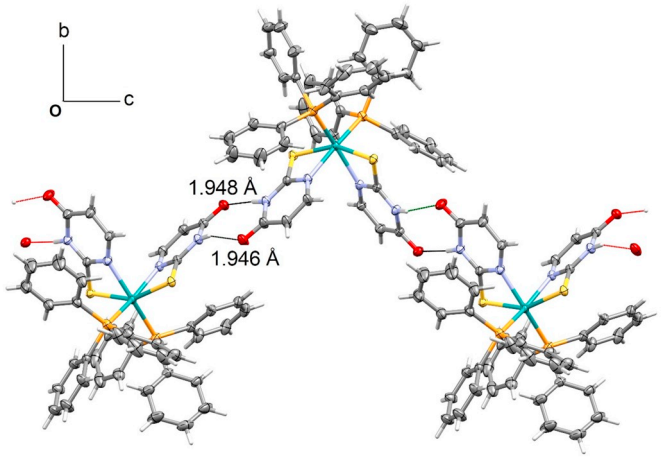

Fig. 2. N-H…O Bifurcated intermolecular H-bonding occurring in complex **1**, stabilizing the crystal self-assembly.

All four complexes are neutral, presenting low molar conductivity values (5–7 $\Omega^{-1}cm^2mol^{-1}$, in DMSO) [50]. The elementary analysis confirms the stoichiometric ratio of 2:1 of thiouracil ligand to metal, for all the complexes. Both 2TU and 6m2TU ligands are coordinated in a similar way, involving the N−S atoms as monoanionic. Further evidence for this behavior was observed by $^{31}P\{^1H\}$ NMR data, showing a singlet in the region of 52–49 ppm for all four compounds (Table 1). This clearly suggests the same stereochemistry around the Ru(II) center for **1–4**. As the phosphorus atoms of the chelating dppb ligand adopt a *cis* configuration, it is expected that the two PPh_3 ligands also adopt the same configuration. Comparing complexes **1** and **3** (with 2TU) and **2** and **4** (with 6m2TU), it can be observed that the chemical shift values for those with 2TU occurs in the lower field region compared to the complexes presenting the 6m2TU ligand. There is a strong indication that the presence of a methyl group at position 6 (see Scheme 1) makes the N-heterocyclic atom of the ligand 6m2TU richer in the electronic density than that one of the 2TU ligand. This contributes to an increase in the electron density in the N-Ru-P bond axis, shielding the phosphorus atom *trans* to nitrogen N1, in complexes **2** and **4**. In addition, it should be emphasized that the ^{31}P NMR, as well as UV–Vis techniques were used to evaluate the stability of the complexes, in which the four compounds showed to be stable in 24, 48 and 72 h (Figs. S28-S39). The effect of the chemical shift under different phosphines was also investigated. For instance, the complexes with the same phosphine ligand, **1** and **2** (with PPh_3) or **3** and **4** (with dppb). It is observed that the complexes with PPh_3 as ligand present more unshielded phosphorus atoms than those ones containing the dppb as ligand. This behavior can be supported comparing the pKa values of PPh_3 (pKa = 2.73) and dppb (pKa = 4.72) [51,52], which agrees with the electrochemical data presented in Table 1, in which the dppb ligand is a better electronic donor than the triphenylphosphine one.

In fact, the electrochemical study revealed similar stereochemistry occurring in all complexes, given that the redox potentials occur in the same region as the voltammogram (Table 1, Figs. S21–24). The electrochemical potential values are lower for complexes presenting 6m2TU as ligand (pKa = 8.20) and this aspect can be explained due to a methyl group at position 6, acting as the electron donor. On the other hand, the highest electrochemical potential values occur for compounds with 2TU ligand which are more acid (pKa = 7.75) than the 6m2TU ligand. As can be seen in Table 1, the complexes containing the dppb ligand present their oxidation potential at a lower value than those containing the PPh_3 ligand.

The infrared studies were carried out to analyze the main changes related to the free ligand [53]. One of the most important pieces of information refers to the position of the carbonyl group stretching vibration. The $\nu C=O$ bands of the 2TU and 6m2TU ligands present values of 1711 and 1674 cm^{-1}, respectively. In the complexes, the $\nu C=O$ stretching vibration was shifted to lower frequencies, concerning the free ligands with a variation of only 23, 15, 37 and 29 cm^{-1} for **1**, **2**, **3** and **4**, respectively. In all cases, the small variation cannot be assigned to the C=O group coordination. The band assignments are summarized in Table S1.

The accurate mass and fragmentation of these complexes were analyzed by high resolution mass spectrometry (HRMS) (see Supplementary information). For complex **1,** the experimental data occur at 880.0792 Da, while the theoretical one is 880.0803 Da for $[M-H]^+$ species . The fragmentations and formation of intermediate molecules were observed during the experiment . The identification of these signals at 617.9859 Da and 753.0911 Da suggests the loss of PPh_3 and the 2TU ligand, respectively, in complex **1**. Furthermore, adducts with water or acetonitrile molecules were also observed. This same behavior is also observed in complexes **2–4**.

The crystal structure obtained by XRD confirmed the coordination of two molecules of thiouracil derivatives per ruthenium(II), and the stereochemistry of the compounds were also confirmed (Fig. 1). The data collections and experimental details for complexes 1-4 are summarized in Table 2. As can be seen, the 2-thiouracil derivatives are coordinated as bidentate ligands *via* S and N(1), with the sulfur atom *trans* to other sulfur atoms of the adjacent ligand, and the nitrogen (N1) atom located is found trans to phosphorus. The same stereochemistry of all complexes are in agreement with $^{31}P\{^1H\}$ NMR data, as well as the Ru(II) compounds previously reported [17,54].

An important trend which can be highlighted is that the bond lengths of Ru−N1 and Ru-N1' are larger in complexes with the 6m2TU ligand than in complexes with the 2TU ligand (Table 3). A plausible explanation for this behavior is the steric hindrance provided by the methyl attached at position 6 of 6m2TU. Moreover, the Ru−P distances in complexes **2** and **4** (with the dppb ligand) are shorter than those determined in complexes **1** and **3** (with the PPh_3 ligand). In such a situation, this behavior may be warranted due to the chelate effect of dppb, keeping the ligand strongly coordinated to the metal center. In addition, bond distances of the 2TU and 6m2TU free ligands are slightly different due to the metal coordination [55]. It can be observed that the C2-S2 bond lengths increased in the complexes, adopting a single bond character, and the N1-C2 bond distances are shorter in the complexes, presenting a double bond character. The coordinated 2-thiouracil derivatives are negatively charged with electron delocalization on the S2···C2···N1 atoms.

All the complexes present strong H-bonds that play an important role in stabilizing the crystal packing and conformation of complexes (see Table 4). All intermolecular contacts were mapped by Hirshfeld analysis (Fig. S26), revealing the presence of short contacts around non-coordinated moiety (N3-H3 and C4═O4) of 2-thiouracil derivatives. As

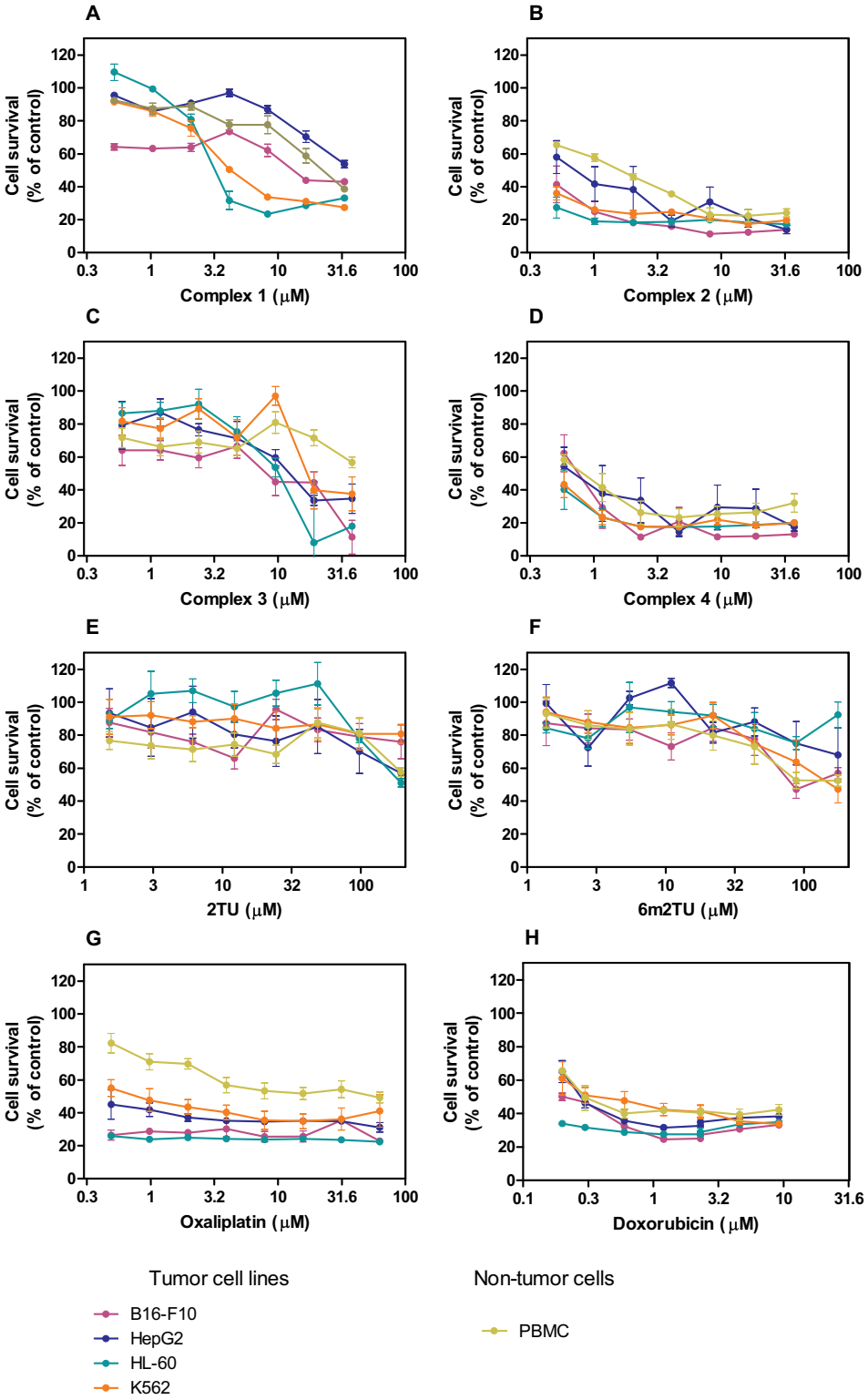

Fig. 3. Cell survival curves obtained from three independent experiments performed in duplicate and measured by alamar blue assay after 72 h of incubation. Tumor cells: B16-F10 (mouse melanoma), HepG2 (human hepatocellular carcinoma), HL-60 (human promyelocytic leukemia) and K562 (human chronic myelocytic leukemia). Non-tumor cell: PBMC (human peripheral blood mononuclear cells activated with concanavalin A – human lymphoblast).

can be seen by X-ray analysis in all structures, the O4 atom is involved in a strong H-bond. As a consequence, the C4═O4 bond lengths can be observed which are slightly longer compared with free ligands. Thus, this aspect can be attributed due to the effect of strong hydrogen bonds involving the N-H…O atom to form a ring type $\mathbf{R_2^2(8)}$ graph-set motif. In Fig. 2, the N-H…O interactions link the molecules of complex **3** in an infinite chain along the *c* axis. This kind of molecular synthon occurs for all structures, except the cis-$[Ru(PPh_3)_2(6m2TU)_2]$ complex, given that the carbonyl group is strongly H-bonded to a methanol molecule. Therefore, all complexes are able to be held strongly by intermolecular H-bonds, which may contribute to the interaction of these molecules with macromolecular targets.

Table 5
Cytotoxic activity (IC_{50} values) for complexes **1–4.**

Compounds	IC_{50} in μM				
	B16-F10	HepG2	HL-60	K562	PBMC
1	25.81	> 28.41	3.42	12.75	> 28.41
	21.00–33.21		3.40–4.89	6.56–24.82	
2	0.81	0.98	0.01	0.20	2.54
	0.64–1.24	0.37–2.34	0.01–0.09	0.10–0.50	2.23–3.86
3	9.89	14.13	17.00	11.91	> 26.71
	5.73–17.09	10.00–20.06	11.38–25.39	9.87–14.37	
4	1.34	0.81	0.15	0.32	1.29
	0.82–1.56	0.34–2.12	0.09–0.47	0.18–0.79	0.67–2.36
2TU	> 195.2	> 195.2	> 195.2	> 195.2	> 195.2
6m2TU	> 175.8	> 175.8	> 175.8	> 175.8	> 175.8
Oxaliplatin	0.05	1.00	0.54	1.23	11.27
	0.03–0.07	0.23–2.33	0.43–1.28	0.34–2.34	3.25–18.38
Doxorubicin	0.02	0.02	0.08	0.13	4.83
	0.01–0.05	0.01–0.06	0.03–0.12	0.05–0.19	2.34–6.93

Table 6
Selectivity index (SI) of compounds **1–4.**

Compounds	SI			
	B16-F10	HepG2	HL-60	K562
1	> 1.1	N.d.	> 8.3	> 2.2
2	3.1	2.6	254	12.7
3	> 2.7	> 1.9	> 1.6	> 2.2
4	1.0	1.6	8.6	4
Oxaliplatin	225.4	11.3	20.9	9.2
Doxorubicin	241.5	241.5	60.4	37.2

3.1. Cytotoxicity of complexes *1–4*

The evaluation of the cytotoxic activity of complexes **1–4** was analyzed against four tumor cell lines and one non-tumor cell, using the alamar blue assay after 72 h incubation (Fig. 3). Table 5 shows the IC_{50} values obtained for each complex. Complexes **2** and **4**, which contain the 6m2TU ligand, exhibited potent cytotoxicity in relation to complexes **1** and **3**, and interestingly, they are the compounds that have the highest K_b values with DNA and BSA. Compared with the positive controls, oxaliplatin and doxorubicin, complexes **2** and **4** present comparable values, revealing that both complexes present promising antitumor applicability. Complex **2** presented IC_{50} values ranging from 0.01 to 0.98 μM for the HL-60 and HepG2 tumor cell lines, and complex **4** presented IC_{50} values ranging from 0.15 to 1.34 μM for the HL-60 and B16-F10 tumor cell lines, respectively. Oxaliplatin presented IC_{50} values ranging from 0.05 to 1.23 μM for the B16-F10 and K562 tumor cell lines, and doxorubicin presented IC_{50} values ranging from 0.02 to 0.13 μM for the B16-F10 and K562 tumor cell lines, respectively. The ligands 2TU (IC_{50} > 195.2) and 6m2TU (IC_{50} > 175.8) were not cytotoxic at the experimental concentrations tested. Regarding the selectivity between tumor cells *versus* non-tumor cells, complexes **2** and **4** showed 254 and 8.6 fold more potent cytotoxicity in HL-60 than PBMC, respectively (Table 6). Indeed, complex **2** is the most selective against HL-60, presenting promising results compared with the clinically useful chemotherapy oxaliplatin and doxorubicin.

Data are presented as IC_{50} values in μM and their 95% confidence interval obtained by nonlinear regression from three independent experiments performed in duplicate, measured by Alamar blue assay after 72 h incubation. Oxaliplatin and doxorubicin were used as positive controls. The 2-thiouracil (2TU) and 6-methyl-2-thiouracil (6m2TU) ligands were also assessed. Tumor cells: B16-F10 (mouse melanoma), HepG2 (human hepatocellular carcinoma), HL-60 (human promyelocytic leukemia) and K562 (human chronic myelocytic leukemia). Non-tumor cell: PBMC (human peripheral blood mononuclear cells activated with concanavalin A – human lymphoblast).

Data presented in the SI were calculated using the following formula: SI = IC_{50}[non-tumor cells]/IC_{50}[tumor cells]. Tumor cells: B16-F10 (mouse melanoma), HepG2 (human hepatocellular carcinoma), HL-60 (human promyelocytic leukemia) and K562 (human chronic myelocytic leukemia). Non-tumor cell: PBMC (human peripheral blood mononuclear cells activated with concanavalin A – human lymphoblast). N.d. Not determined.

Ruthenium complexes with different ligands were reported as potent cytotoxic agents. Interestingly, complexes **2** and **4** presented higher potency than previously synthesized ruthenium complexes. As a comparison, the ruthenium complexes containing 2-hydroxy-5-nitrophenyl) (pyrrolidin-1-yl)methanethione showed IC_{50} values above 40 μM in human cervical carcinoma (HeLa) and breast adenocarcinoma (MCF-7) cell lines [56]. The ruthenium-based 5-fluorouracil complex presented cytotoxicity for different tumor cells, especially with the IC_{50} value of 2.6 μM for HL-60 cells and a SI of 2.2 (HL-60 *versus* PBMC) [8], while a Ru(II)-thymine complex showed IC_{50} value of 1.4 μM for HL-60 cells and a SI of 1.2 (HL-60 *versus* PBMC) [10]. In addition, a ruthenium complex with xanthoxylin displayed IC_{50} value of 6.6 μM for HL-60 cells and a SI of 0.7 (HL-60 *versus* PBMC) [57]. Complexes **2** and **4** studied here showed an IC_{50} value of 0.01 and 0.15 μM for HL-60 cells and SI of 254 and 8.6 (HL-60 *versus* PBMC), respectively, showing that they are promising antitumor drug candidates.

3.2. Interactions of complexes 1–4 with CT-DNA by UV–Vis and DNA fragmentation of complexes 2 and 4 in HL-60 cells

To verify that complexes **1–4** interact with CT-DNA, a study *via* spectroscopic titration was carried out. Under the presence of the Ru(II) complexes **1–4**, a CT-DNA hypochromism was observed in the range of approximately 15–25% (Table 5), suggesting a moderate interaction between the complexes and DNA, which is seen by DNA binding constant (K_b) values of complexes **1–4** [Eq. (1)].

$$[CT-DNA]/(\varepsilon_a-\varepsilon_f) = [CT-DNA]/(\varepsilon_b-\varepsilon_f) + 1/K_b(\varepsilon_b-\varepsilon_f) \quad (1)$$

in which [CT-DNA] is the concentration of CT-DNA in base pairs, ε_a is the ratio of the absorbance/[Ru(II) complex], ε_f is the extinction coefficient of the free Ru(II) complex, and ε_b is the extinction coefficient of the complex in the fully bound form. The ratio of the slope to the intercept in the plot of [CT-DNA]/(ε_a–ε_f) *vs.* [CT-DNA] gives the value of K_b, which was the calculated absorption band (λ_{max}) at around 320 nm. The electronic spectra obtained for all complexes are similar (Fig. S27). The K_b values are around $10^4\,M^{-1}$ (2 > 4 > 1 > 3), indicating a moderate interaction with CT-DNA (which probably involve hydrogen bonds), when compared with the K_b value of a classic DNA intercalator, such as ethidium bromide (K_b $10^6\,M^{-1}$) [58]. The similar magnitude of

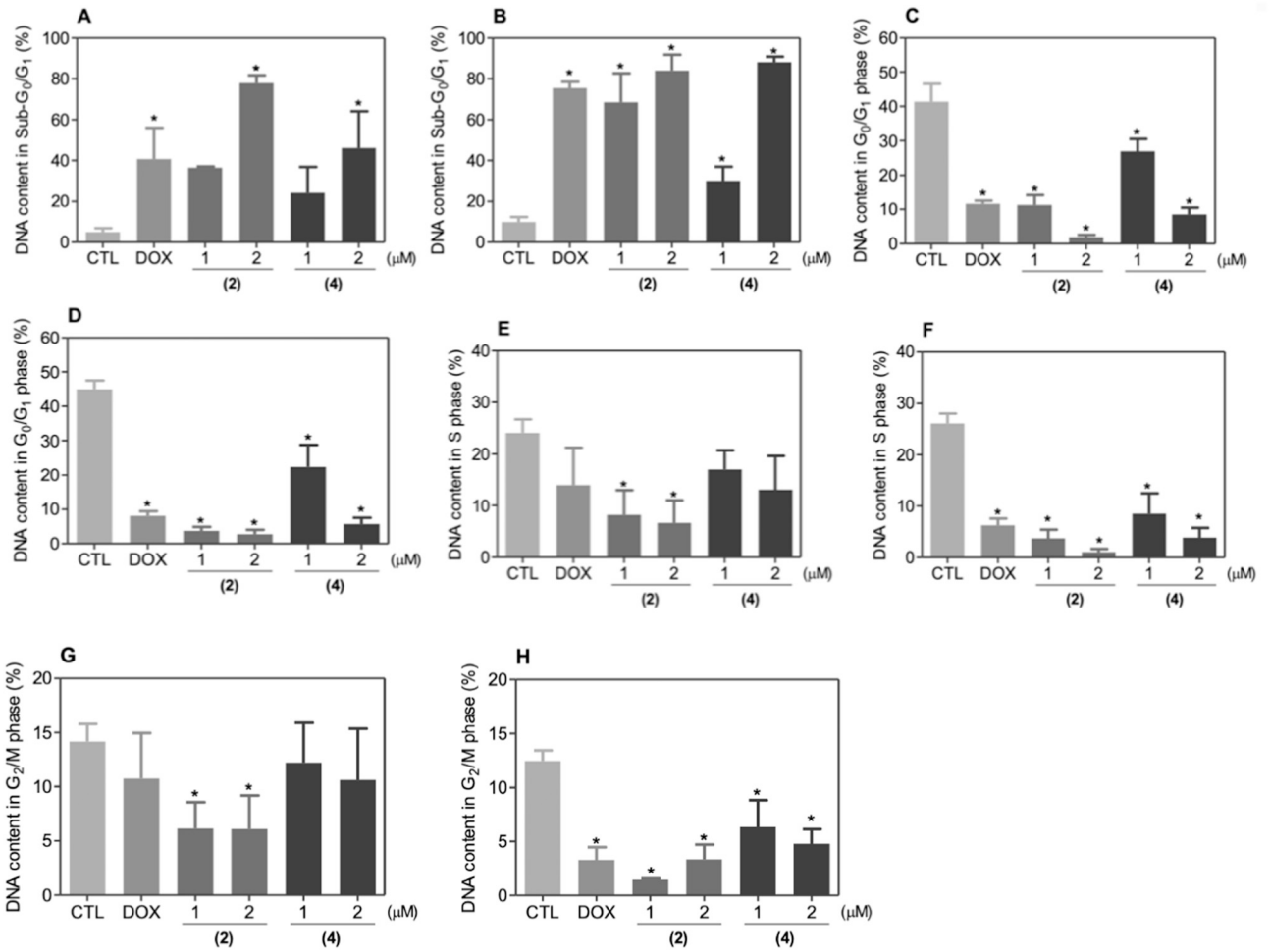

Fig. 4. Effect of complexes **2** and **4** in the cell cycle distribution of HL-60 cells after 12 (**A**, **C**, **E** and **G**) and 24 (**B**, **D**, **F** and **G**) h of treatment. Data are presented as the means ± S.E.M. of at least three independent experiments performed in duplicate. The negative control (CTL) was treated with the vehicle (0.2% DMSO) used for diluting the complexes. Doxorubicin (DOX, 1 μM) was used as the positive control. Ten thousand events were evaluated per experiment and cellular debris was omitted from the analysis. * $P < 0.05$ compared with the negative control by ANOVA, followed by the Student Newman-Keuls Test.

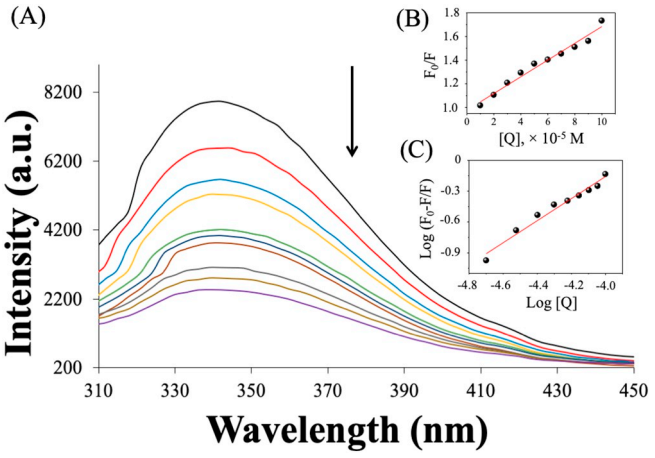

Fig. 5. (A) View of fluorescence quenching of BSA with increasing concentration of complex **1**, (**B**) Stern-Volmer plots and (**C**) log(F_0−F)/F *vs.* log [Q].

K_b found for **1–4** is comparable with those metal complexes with non-covalent interactions with DNA reported in the literature (K_b around 10^4–10^5 M^{-1}) [59,60].

The DNA fragmentation and cell cycle distribution was performed in HL-60 cells treated with complexes **2** and **4** by flow cytometry through the incorporation of propidium iodide after 12 and 24 h of treatment (Fig. 4). All the DNA that was subdiploid (sub-G_0/G_1) was considered fragmented. Both complexes increased the DNA fragmentation. After 12 h of treatment, complex **2** led to 77.9% of DNA fragmentation at a concentration of 2 μM, while complex **4** caused 46.2% (compared to 4.9% of the negative control). After 24 h of treatment, complex **2** led to 68.5 and 84.0% of DNA fragmentation at concentrations of 2 and 4 μM, and complex **4** caused 30.2 and 88.2% (compared to 9.9% of the negative control), respectively. All phases of the cell cycle (G_0/G_1, S and G_2/M) decreased after treatment with these complexes. Doxorubicin also induced DNA fragmentation.

The increase in the DNA fragmentation represents cell death. In previous studies, augments of DNA fragmentation were associated with cell death by apoptosis as observed by Oliveira et al. [61], who reported a novel platinum complex containing a piplartine derivative with enhanced cytotoxicity that caused oxidative stress and triggers apoptotic cell death by ERK/p38 pathway in HL-60 cells. The ruthenium-based 5-fluorouracil complex also caused DNA fragmentation accompanied by the induction of caspase-mediated apoptosis in human colon carcinoma HCT116 cells [8]. HeLa cell treatment with a ruthenium(II)-arene complex and an isoquinoline-3-carboxylic acid ligand demonstrated a relationship between the percentage of cells in apoptosis and an increase in cells with DNA fragmentation [62]. The ruthenium complexes with piplartine also induced internucleosomal DNA fragmentation and were able to cause caspase-dependent and mitochondrial intrinsic

Table 7
Stern-Volmer quenching constant (K_{sv}, M^{-1}), bimolecular quenching constant (k_q, $M^{-1}\,s^{-1}$), binding constant (K_b, M^{-1}) and binding site (*n*).

	$K_b \times 10^4$ (CT-DNA)	T (K)	Ksv × 10^3	$k_q \times 10^{11}$	Kb (BSA)	*n*
(1)	(2.9 ± 0.3)	298	(2.7 ± 0.2)	4.38	(2.1 ± 0.1) × 10^2	0.66
		310	(2.9 ± 0.2)	4.75	(4.1 ± 0.7) × 10^2	0.51
(2)	(5.4 ± 0.7)	298	(4.3 ± 0.1)	7.02	(1.7 ± 0.1) × 10^3	0.95
		310	(4.8 ± 0.1)	7.87	(8.1 ± 0.9) × 10^3	0.81
(3)	(2.3 ± 0.2)	298	(6.6 ± 0.3)	10.60	(2.2 ± 0.5) × 10^2	0.64
		310	(7.4 ± 0.1)	11.95	(2.8 ± 0.3) × 10^2	0.61
(4)	(3.6 ± 0.2)	298	(6.9 ± 0.1)	11.21	(0.98 ± 0.02) × 10^3	1.05
		310	(7.7 ± 0.1)	12.68	(1.2 ± 0.2) × 10^3	0.84

Table 8
Thermodynamic parameters of interaction between ruthenium complexes **1–4** and BSA.

	T (K)	ΔG° (kJ mol^{-1})	ΔH° (kJ mol^{-1})	ΔS° (J $mol^{-1}\,K^{-1}$)
(1)	298	−13.22	−43.40	−101.26
	310	−15.50		−89.98
(2)	298	−18.44	−99.79	−272.96
	310	−23.21		−247.03
(3)	298	−13.36	−15.42	−6.91
	310	−14.52		−2.90
(4)	298	−17.06	−17.36	−1.00
	310	−18.34		−3.14

apoptosis in HCT116 cells by the oxidative stress-mediated pathway [63]. The ruthenium complex with xanthoxylin caused the S-phase arrest with internucleosomal DNA fragmentation, and led to ERK1/2-mediated apoptosis in HepG2 cells through an oxidative stress- and p53-independent pathway [57].

3.3. Bovine serum albumin binding

The interaction of complexes with bovine serum albumin (BSA) was investigated. The fluorescence of BSA free is a result of the presence of tryptophan and tyrosine residues. Changes in the BSA emission spectra can be related with conformational changes in the structure of this protein. Considering that albumin is partly responsible for the transport of endogenous and exogenous substances through the bloodstream [64], the interaction of the Ru(II) complexes with albumin needs to be investigated. Therefore, the compound binding to albumin may influence its distribution, pharmacokinetic property, or even change the transportation paths through the body [65]. Based on these aspects, to investigate if the ruthenium/thiouracil complexes can interact with BSA enables us to understand the possible bioavailability of the complexes. The interaction with BSA was investigated by the quenching of the fluorescence after incubation with complexes in different concentrations. Fig. 5 shows the fluorescence emission spectra obtained for BSA in the presence of complex **1**, varying its concentration.

It can be observed that the fluorescence intensity of BSA decreased in the presence of the complexes, indicating interaction with the protein. To gain more insight into the type of interaction, the Stern-Volmer (K_{sv}) constant was calculated (Table 7), using the Stern-Volmer Eq. (2), from the plots of F_0/F *versus* [Q].

$$F_0/F = +k_q\tau_0[Q] = +K_{sv}[Q] \quad (2)$$

where, F_0 and F are the fluorescence of BSA in the absence and presence of complexes, k_q is the bimolecular quenching constant and τ_0 (6.2 ns) is the average lifetime of the fluorophore in the absence of quencher, [Q] is the concentration of complexes and K_{sv} is the Stern-Volmer constant [66]. According to the results, the K_{sv} constants increased with the increase in temperature, which indicates the dynamic quenching. At a higher temperature, the diffusion coefficients increase because of the faster diffusion and hence larger amounts of collisional quenching [67]. Moreover, the values of the bimolecular quenching constant (k_q) obtained from K_{sv} and τ_0 (6.2 ns) are in the range of 4.38–12.68 × $10^{11}\,M^{-1}\,s^{-1}$, which are higher than the maximum value for dynamic quenching (2.0 × $10^{10}\,M^{-1}\,s^{-1}$) [68]. Thus, this is indicative that the dynamic and static quenching mechanism occurs simultaneously. The binding constant (K_b) and number of binding sites (*n*) were determined using the Scatchard Eq. (3) [67]:

$$\log\frac{(F_0 - F)}{F} = \log K_b + n\log[Q] \quad (3)$$

As shown in Table 7, the K_b values are within the range of 10^2 to $10^3\,M^{-1}$, which indicates that the complexes interact more weakly with BSA than other ruthenium(II) complexes previously reported, with binding constants ranging from 10^5 to $10^8\,M^{-1}$ [69]. The values of *n* indicate that the complexes interact at only one binding site.

Finally, to identify the type of interaction forces that are involved between the complexes and BSA, some thermodynamic parameters such as free energy changes (ΔG°), enthalpy changes (ΔH°) and entropy changes (ΔS°) were determined, using the following Eqs. (4) and (5):

$$\ln\left(\frac{K_{b1}}{K_{b2}}\right) = \left(\frac{1}{T_1} - \frac{1}{T_2}\right) \times \frac{\Delta H°}{R} \quad (4)$$

$$\Delta G° = -RT\ln K_b = \Delta H° - T\Delta S° \quad (5)$$

where K_{b1} and K_{b2} are the binding constants in temperature T_1 and T_2 and R is the gas constant [69].

The negative ΔG° values (Table 8) indicate that the interaction between Ru(II)-thiouracil complexes and BSA occurs by spontaneous process. In addition, the negative ΔH° and ΔS° values suggest the involvement of van der Waals forces and hydrogen bonding interactions [70], which is in agreement with the structural characteristic of complexes **1–4** and possibilities to form intermolecular contacts, such as those observed by Hirshfeld surface analysis.

4. Conclusions

In summary, four new ruthenium(II) complexes containing phosphines and thiouracil derivatives were obtained. The stereochemistry, intermolecular interactions and cytotoxicity of the complexes were studied. The crystal structures were determined for all complexes and showed that all complexes are neutral. The phosphorus atoms of dppb or PPh_3 ligands are in *cis* configuration relative to each other, and *trans* to nitrogen atom (N1) of the thiouracil derivative, such as what was suggested by the $^{31}P\{^1H\}$ NMR experiment. In addition, the two thiouracil ligands show the *trans*-S atom to another S atom. Studies on complex/DNA interaction by spectroscopic titrations have shown that complexes **1–4** exhibit moderate binding to DNA, as observed by the values of K_b binding constants. The complexes showed weak interactions with BSA by a dynamic and static quenching and with the involvement of van der Waals forces and hydrogen bonding interactions. Furthermore, the IC_{50} values against tumor cells for the complexes are lower than the IC_{50} values against non-tumor cells that are desired. Complexes **2** and **4**, with 6m2TU ligands, showed to be more active

than complexes **1** and **3**, with 2-TU ligands. Therefore, the work reported here showed promising antitumor candidates with 6m2TU ligands that will be studied in detail as a potent chemotherapeutic agent.

Declaration of Competing Interest

The authors declare that they have no conflict of interests.

Acknowledgements

We would like to thank the Brazilian Research Agencies: CNPq, CAPES, FAPEMIG, FAPESP and FAPESB. R.S. Correa would like to thank the financial support provided by CNPq (grant 403588/2016-2 and 308370/2017-1) and FAPEMIG (APQ-01674-18). K. M. Oliveira is thankful to CAPES for a postdoctoral fellowship. The authors are thankful to Professor Carlos Bloch Jr. for helping us to determine the high resolution mass spectrometry data. The authors would also like to thank the Laboratório Multiusuário de Caracterização de Moléculas (UFOP) for the excellent Nuclear Magnetic Resonance service.

Appendix A. Supplementary data

Crystallographic Information Files (CIFs) under CCDC reference numbers 1,880,931, 1,880,932, 1,880,933 and 1,880,934 for **1**, **2**, **3** and **4,** respectively, and PDF file of Table S1. Figs. S1 to S12 ($^{31}P\{^{1}H\}$, $^{13}C\{^{1}H\}$ and ^{1}H NMR spectra for complexes **1–4**), S13 to S16 (HRMS spectra for complexes **1–4**), S17 to S20 (Infrared spectra for complexes **1–4**), S21 to S24 (Electrochemical experiment for complexes **1–4**), S25 (UV–Vis spectra for complexes **1–4**), S26 (Hirshfeld surface and fingerprint plot for complexes **1–4**), S27 (CT-DNA UV–Vis titration spectra for complexes **1–4**), S28 to S39 (Stability studies for complexes **1–4**).Table S1 (Infrared assignment for complexes **1–4**). Supplementary data to this article can be found online at https://doi.org/10.1016/j.jinorgbio.2019.110751.

References

[1] J.-X. Liang, H.-J. Zhong, G. Yang, K. Vellaisamy, D.-L. Ma, C.-H. Leung, J. Inorg. Biochem. 177 (2017) 276–286.
[2] I. de Aguiar, A. Tavares, A.C. Roveda, A.C.H. da Silva, L.B. Marino, É.O. Lopes, F.R. Pavan, L.G.F. Lopes, D.W. Franco, Eur. J. Pharm. Sci. 70 (2015) 45–54.
[3] B.V. Silva, B.N.M. Silva, Med. Chem. 13 (2017) 110–126.
[4] A. Peruzzo, J. McClean, P. Shadbolt, M.-H. Yung, X.-Q. Zhou, P.J. Love, A. Aspuru-Guzik, J.L. O'Brien, Nat. Commun. 5 (2014) 4213.
[5] E. Meggers, G.E. Atilla-Gokcumen, K. Gründler, C. Frias, A. Prokop, Dalt. Trans. (2009) 10882–10888.
[6] L. Zhang, P. Carroll, E. Meggers, Org. Lett. 6 (2004) 521–523.
[7] R.S. Correa, K.M. De Oliveira, F.G. Delolo, A. Alvarez, R. Mocelo, A.M. Plutin, M.R. Cominetti, E.E. Castellano, A.A. Batista, J. Inorg. Biochem. 150 (2015) 63–71.
[8] V.R. Silva, R.S. Corrêa, L. de S. Santos, M.B.P. Soares, A.A. Batista, D.P. Bezerra, Sci. Rep. 8 (2018) 288.
[9] R.S. Correa, V. Freire, M.I.F. Barbosa, D.P. Bezerra, L.M. Bomfim, D.R.M. Moreira, M.B.P. Soares, J. Ellena, A.A. Batista, New J. Chem. 42 (2018) 6794–6802.
[10] M. de Souza Oliveira, Á.A.D. de Santana, R.S. Correa, M.B.P. Soares, A.A. Batista, D.P. Bezerra, Int. J. Mol. Sci. 19 (2018) 1609.
[11] K.M. Oliveira, R.S. Corrêa, M.I.F. Barbosa, J. Ellena, M.R. Cominetti, A.A. Batista, Polyhedron 130 (2017) 108–114.
[12] B.N. Cunha, L. Colina-Vegas, A.M. Plutín, R.G. Silveira, J. Honorato, K.M. Oliveira, M.R. Cominetti, A.G. Ferreira, E.E. Castellano, A.A. Batista, J. Inorg. Biochem. 186 (2018) 147–156.
[13] M.I.F. Barbosa, R.S. Corrêa, L.V. Pozzi, É. de O. Lopes, F.R. Pavan, C.Q.F. Leite, J. Ellena, S. de P. Machado, G. Von Poelhsitz, A.A. Batista, Polyhedron 85 (2015) 376–382.
[14] E.R. dos Santos, M.A. Mondelli, L.V. Pozzi, R.S. Corrêa, H.S. Salistre-de-Araújo, F.R. Pavan, C.Q.F. Leite, J. Ellena, V.R.S. Malta, S.P. Machado, A.A. Batista, Polyhedron 51 (2013) 292–297.
[15] E.R. Dos Santos, R.S. Corrêa, J.U. Ribeiro, A.E. Graminha, J. Ellena, H.S. Selistre-de-Araujo, A.A. Batista, J. Coord. Chem. 69 (2016) 3518–3530.
[16] E.R. dos Santos, R.S. Corrêa, L.V. Pozzi, A.E. Graminha, H.S. Selistre-de-Araújo, F.R. Pavan, A.A. Batista, Inorganica Chim. Acta. 463 (2017) 1–6.
[17] B.A.V. Lima, A.E. Graminha, A. Kuznetsov, J. Ellena, F.R. Pavan, C.Q.F. Leite, A.A. Batista, J. Braz. Chem. Soc. 27 (2016) 30–40.
[18] M.I.F. Barbosa, R.S. Correa, T.M. Bastos, L.V. Pozzi, D.R.M. Moreira, J. Ellena, A.C. Doriguetto, R.G. Silveira, C.R. Oliveira, A.E. Kuznetsov, V.S. Malta, M.B.P. Soares, A.A. Batista, New J. Chem. 41 (2017) 4468–4477.
[19] R.S. Corrêa, M.M. Da Silva, A.E. Graminha, C.S. Meira, J.A.F. Dos Santos, D.R.M. Moreira, M.B.P. Soares, G. Von Poelhsitz, E.E. Castellano, C. Bloch, M.R. Cominetti, A.A. Batista, J. Inorg. Biochem. 156 (2016) 153–163.
[20] E. Meggers, Chem. Commun. (2009) 1001–1010.
[21] A.N. Boynton, L. Marce, A.J. Mcconnell, J.K. Barton, 2 (2017).
[22] M.S. de Camargo, R.A. De Grandis, M.M. da Silva, P.B. da Silva, M.M. Santoni, C.E. Eismann, A.A. Menegário, M.R. Cominetti, C.F. Zanelli, F.R. Pavan, A.A. Batista, BioMetals 32 (2019) 89–100.
[23] J. Li, M. Tian, Z. Tian, S. Zhang, C. Yan, C. Shao, Z. Liu, Inorg. Chem. 57 (2018) 1705–1716.
[24] V. Prachayasittikul, R. Pingaew, C. Nantasenamat, S. Prachayasittikul, S. Ruchirawat, V. Prachayasittikul, Drug Des. Devel. Ther. 8 (2014) 1089–1096.
[25] V.S. Velozo-Sá, L.R. Pereira, A.P. Lima, F. Mello-Andrade, M.R.M. Rezende, R.M. Goveia, W.C. Pires, M.M. Silva, K.M. Oliveira, A.G. Ferreira, J. Ellena, V.M. Deflon, C.K. Grisolia, A.A. Batista, E.P. Silveira-Lacerda, Dalt. Trans. 48 (2019) 6026–6039.
[26] F. Basolo, R.G. Pearson, Mechanisms of Inorganic Reactions, John Wiley & Sons, Ltd, New York, 1958.
[27] S. Kitagawa, Y. Nozaka, M. Munakata, S. Kawata, Inorganica Chim. Acta. 197 (1992) 169–175.
[28] F. Shaheen, A. Badashah, M. Gielen, L. Marchio, D. de Vos, M. Kaleem Khosa, Appl. Organomet. Chem. 21 (2007) 626–632.
[29] J.S. Casas, E.E. Castellano, M.S. García-Tasende, A. Sánchez, J. Sordo, E.M. Vázquez-López, J. Zukerman-Schpector, J. Chem. Soc. Dalt. Trans. (1996) 1973–1978.
[30] F. Sce, G. Beobide, O. Castillo, I. de Pedro, S. Pérez-Yáñez, E. Reyes, CrystEngComm 19 (2017) 6039–6048.
[31] K. Paizanos, D. Charalampou, N. Kourkoumelis, D. Kalpogiannaki, L. Hadjiarapoglou, A. Spanopoulou, K. Lazarou, M.J. Manos, A.J. Tasiopoulos, M. Kubicki, S.K. Hadjikakou, Inorg. Chem. 51 (2012) 12248–12259.
[32] C.S.W. Harker, E.R.T. Tielink, M.W. Whitehouse, Inorganica Chim. Acta. 181 (1991) 23–30.
[33] V.I. Balas, I.I. Verginadis, G.D. Geromichalos, N. Kourkoumelis, L. Male, M.B. Hursthouse, K.H. Repana, E. Yiannaki, K. Charalabopoulos, T. Bakas, S.K. Hadjikakou, Eur. J. Med. Chem. 46 (2011) 2835–2844.
[34] N.N. Golovnev, M.S. Molokeev, S.N. Vereshchagin, V.V. Atuchin, M.Y. Sidorenko, M.S. Dmitrushkov, Polyhedron 70 (2014) 71–76.
[35] Z.R. Pan, Y.C. Zhang, Y.L. Song, X. Zhuo, Y.Z. Li, H.G. Zheng, J. Coord. Chem. 61 (2008) 3189–3199.
[36] J.R. Lusty, J. Peeling, M.A. Abdel-Aal, Inorganica Chim. Acta. 56 (1981) 21–26.
[37] M. Ruf, K. Weis, H. Vahrenkamp, 1669 (1997) 2130–2137.
[38] K. Yamanari, M. Kida, A. Fuyuhiro, M. Kita, S. Kaizaki, Inorganica Chim. Acta. 332 (2002) 115–122.
[39] M.A. Esteruelas, J. García-Raboso, M. Oliván, Inorg. Chem. 51 (2012) 9522–9528.
[40] S. Chakraborty, R.H. Laye, P. Munshi, R.L. Paul, M.D. Ward, G. Kumar Lahiri, J. Chem. Soc. Dalt. Trans. (2002) 2348–2353.
[41] C. Ma, G. Tian, R. Zhang, J. Organomet. Chem. 691 (2006) 2014–2022.
[42] G. Stephson, T.A. Wilkinson, J. Inorg. Nucl. Chem. 28 (1966) 945.
[43] G.M. Sheldrick, Acta Crystallogr. Sect. C Struct. Chem. 71 (2015) 3–8.
[44] P. Coppens, L. Leiserowitz, D. Rabinovich, Acta Crystallogr. 18 (1965) 1035–1038.
[45] L.J. Farrugia, J. Appl. Crystallogr. 32 (1999) 837–838.
[46] C.F. Macrae, I.J. Bruno, J.A. Chisholm, P.R. Edgington, P. McCabe, E. Pidcock, L. Rodriguez-Monge, R. Taylor, P.A. J. Van De Streek, J. Appl. Crystallogr. 41 (2008) 466–470.
[47] M.A.S.S.K. Wolff, D.J. Grimwood, J.J. McKinnon, M.J. Turner, D. Jayatilaka, CrystalExplorer 3.1, University of Western Australia, Univ. West. Aust, 2012.
[48] Wolfe, G.H. Shimer, T. Meehan, Biochemistry 26 (1987) 6392–6396.
[49] S. Ansar Ahmed, R.M. Gogal, J.E. Walsh, J. Immunol. Methods 170 (1994) 211–224.
[50] W.J. Geary, Coord. Chem. Rev. 7 (1971) 81–122.
[51] J.R. Sowa, R.J. Angelici, Inorg. Chem. 30 (1991) 3534–3537.
[52] M.M. Rahman, H.Y. Liu, K. Eriks, A. Prock, W.P. Giering, Organometallics 8 (1989) 1–7.
[53] L. Grosmaire, J.-L. Delarbre, J. Mol. Struct. 1011 (2012) 42–49.
[54] R.S. Corrêa, M.M. da Silva, A.E. Graminha, C.S. Meira, J.A.F. dos Santos, D.R.M. Moreira, M.B.P. Soares, G. Von Poelhsitz, E.E. Castellano, C. Bloch, M.R. Cominetti, A.A. Batista, J. Inorg. Biochem. 156 (2016) 153–163.
[55] K.N. Jarzembska, M. Kubsik, R. Kamiński, K. Woźniak, P.M. Dominiak, Cryst. Growth Des. 12 (2012) 2508–2524.
[56] M. Das, R. Nasani, M. Saha, S.M. Mobin, S. Mukhopadhyay, Dalton Trans. 44 (2015) 2299–2310.
[57] V.A. Online, Y. Ebrahimipour, M. Torkzadeh, S. Foro, RSC Adv. 5 (2015) 101063–101075.
[58] M. Ganeshpandian, R. Loganathan, E. Suresh, A. Riyasdeen, M.A. Akbarsha, M. Palaniandavar, Dalton Trans. 43 (2014) 1203–1219.
[59] J.R. Lacowicz, Principles of Fluorescence Spectroscopy, Kluver Academic/Plenum Publishers, New York, 1999.
[60] X. Zhao, R. Liu, Z. Chi, Y. Teng, P. Qin, J. Phys. Chem. B 114 (2010) 5625–5631.
[61] K.M. Oliveira, L.-D. Liany, R.S. Corrêa, V.M. Deflon, M.R. Cominetti, A.A. Batista, J. Inorg. Biochem. 176 (2017) 66–76.
[62] P.D. Ross, S. Subramanian, Biochemistry 20 (1981) 3096–3102.
[63] R.R. Kumar, R. Ramesh, J.G. Małecki, New J. Chem. 41 (2017) 9130–9141.
[64] N.C. de Carvalho, S.P. Neves, R.B. Dias, L. de F. Valverde, C.B.S. Sales,

C.A.G. Rocha, M.B.P. Soares, E.R. dos Santos, R.M.M. Oliveira, R.M. Carlos, P.C.L. Nogueira, D.P. Bezerra, Cell Death Dis. 9 (2018) 79.
[65] J.B. LePecq, C. Paoletti, J. Mol. Biol. 27 (1967) 87–106.
[66] N. Shahabadi, S.M. Fili, J. Coord. Chem. 71 (2018) (2018) 16–18.
[67] G.L. Ma, X.D. Bi, F. Gao, Z. Feng, D.C. Zhao, F.J. Lin, R. Yan, D. Liu, P. Liu, J. Chen, H. Zhang, J. Inorg. Biochem. 185 (2018) 1–9.
[68] M. de S. Oliveira, M.I.F. Barbosa, T.B. de Souza, D.R.M. Moreira, F.T. Martins, W. Villarreal, R.P. Machado, A.C. Doriguetto, M.B.P. Soares, D.P. Bezerra, Redox Biol. 20 (2019) 182–194.
[69] K.K. Jovanović, M. Tanić, I. Ivanović, N. Gligorijević, B.P. Dojčinović, S. Radulović, J. Inorg. Biochem. 163 (2016) 362–373.
[70] C.O. D'Sousa, J.H. Araujo, I.R.S. Baliza, R.B. Dias, F. Valverde, M.T.A. Vidal, C.B.S. Sales, G. Rocha, D.R.M. Moreira, M.B.P. Soares, A.A. Batista, D.P. Bezerra, Redox Biol. 20 (2019) 182–194.